Nanotip design for high-resolution terahertz scattering-type scanning near field optical microscopy

Zeliang Zhang[1,2], Pengfei Qi[1,2], Olga Kosavera[1,3] Minghui Deng[1,2], Cheng Gong[1,2*], Lie Lin[1,4], Weiwei Liu[1,2]

[1]Institute of Modern Optics, Nankai University, Tianjin 300350, China;
[2]Tianjin Key Laboratory of Micro-scale Optical Information Science and Technology;
[3]Faculty of Physics, Lomonosov Moscow State University, Leninskie Gory, Moscow 119991, Russia;
[4]Tianjin Key Laboratory of Optoelectronic Sensor and Sensing Network Technology;

*Corresponding author: gongcheng@nankai.edu.cn;

Terahertz (THz) scattering-type scanning near-field optical microscopy (THz s-SNOM) is an important means of studying and revealing material properties at the nanoscale. Nanotip is one of the core components of THz s-SNOM, which has a decisive impact on the resolution of the system. This paper focuses on the theory and design of nanotip, and conducts comprehensive research on it through simulation. The theoretical model is based on full wave numerical simulation and dipole moment analysis which can describe the overall nanotip electromagnetic response under the incident field. A comprehensive design model of nanotips' geometry, sample materials, and incident field is established to significantly improve the near-field couple efficiency and spatial resolution to achieve optimal performance.

Keywords: THz near field microscopy, Nanotip, Full wave numerical simulation

1. Introduction

Terahertz (THz) radiation is located at an important position in the electromagnetic spectrum. THz spectroscopy has been widely applied to resonantly probe collective charge, spin, and lattice oscillations in solids, the rotations of small polar molecules and the structural vibrations of large biomolecules [1–3]. THz imaging has become the distinctive detection technique in biological tissue samples and new materials [4–6]. However, the spatial resolution with conventional optical methods is constrained by the diffraction limit, which obstructs the application and development of THz imaging. Scattering scanning near-field microscopy is a promising scanning probe technique, which conveys near-field dielectric information by nano tips scattering and is detected by conventional far-field detectors [7,8]. The surface charge density of the tip apex is polarized by the incident field, and the surface charge is concentrated to the nanoscale by the tip apex [9,10]. When the nanotip-sample distance reduces to near-field region, the tip scattering field is influenced by the local tip-sample system's dielectric properties. The nanotip-sample system scattering field can be transferred and recorded at the far-field. The dielectric information and surface topography can be recorded simultaneously [11–14].

In the THz s-SNOM system, the spatial resolution and near-field couple efficiency are predominantly determined by the tip geometry, as the nanoscale tips provide the basic near-field environment [15,16]. Nanotips with different performance characteristics have different fabrication processes, including photolithography, electron beam lithography (EBL), and reactive ion etching (RIE). Besides, the dielectric response of the sample surface and incident field intensity and polarization also affect the near-field couple efficiency. This letter comprehensively characterizes the performance improvement for the near-field spatial resolution and near-field couple efficiency induced by nanotips' geometry, nanotip material, sample material, and incident field. The theoretical model is a numerical full wave simulation based on solving Maxwell's equations in the frequency domain [17]. The spatial resolution is dominated by the tip apex radius, tip cone angle and tip-sample distance. The near-field couple efficiency is dominated by the tip geometry and incident field polarization.

The current THz s-SNOM systems are typically constructed with continuous THz sources or photoconductive antennas, which yield THz pulses with low peak power and are unfavorable for enhancing near-field coupling efficiency. Common methods for generating intense THz pulses include optical rectification and femtosecond laser filamentation. The spectral energy distribution of these intense THz sources is primarily centered around 0.5 THz [18,19]. Consequently, this letter concentrates on the design of THz s-SNOM probes within the 0.5 THz range. These intense THz sources typically necessitate the utilization of femtosecond laser amplifiers as their driving light sources, leading to lower repetition rates for these THz sources (The disadvantage of low repetition rate is being overcome) [20]. This simulation method extends the application of such high peak power THz sources in THz s-SNOM.

2. Theoretical model

Full wave numerical simulations offer a distinct advantage in comprehensively characterizing the electromagnetic response of a nanotip illuminated by the THz field. In Full Wave Numerical Simulations, the

electric dipole moment of a charge distribution is defined by the integral expression [21]:

$$\mathbf{p}(t) = \int d^3x' \mathbf{x}' \rho\left(\mathbf{x}', t\right) \tag{1}$$

In equation (1), x' and $\mathbf{x}'$ are the positions where the charge density is evaluated, which describes the electromagnetic response of the nanotips scattering and sample surface scattering. $\rho\left(\mathbf{x}', t\right)$ determines the charge density of the nanotip's apex surface. Charge conservation relates the charge density to the current density by the continuity equation [21,22]:

$$\nabla \cdot \mathbf{J} + \frac{\partial \rho}{\partial t} = 0 \tag{2}$$

J is the current density. The following relation between the electric dipole moment and the current density follows (D is the electric displacement vector, H is the magnetic field intensity, and ω is the angular frequency) [21,22]:

$$\frac{d}{dt}\mathbf{p}(t) = \int d^3x' \mathbf{J}\left(\mathbf{x}', t\right) \tag{3}$$

$$\mathbf{J} = \begin{vmatrix} \mathbf{i} & \mathbf{j} & \mathbf{k} \\ \frac{\partial}{\partial x} & \frac{\partial}{\partial y} & \frac{\partial}{\partial z} \\ H_x & H_y & H_z \end{vmatrix} - (-i\omega \mathbf{D}) \tag{4}$$

As it is shown in equation (3), the electric dipole moment is proportional to the current density. The tip-scattered electric field $E_{focusing}$ is proportional to the complex-valued dipole moment **p(t)**, calculated numerically according to [21,22]:

$$E_{focusing} \propto \mathbf{p}(t) = \int \sigma(\mathbf{r}) \mathbf{r} d\mathbf{r} \tag{5}$$

$$\sigma \propto \mathbf{E} \cdot \mathbf{n} \tag{6}$$

$\sigma(r)$ is the surface charge density, **r** is the nanotips' apex radius, **E** is the electric field vector and **n** is the outward normal to the tip surface.

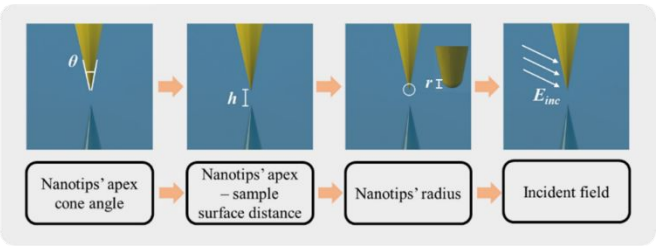

Figure 1. The research process of the nanotip of THz s-SNOM. The research process involves two aspects: the influence of the nanotip's geometry and the incident field on the near-field scattering signal.

This paper focuses on designing a nanotip design method to improve the THz s-SNOM spatial resolution and near-field couple efficiency by solving Maxwell's equations in the frequency (Full Wave Numerical Simulations). The research process of the nanotip aims to achieve high spatial resolution and high near-field couple efficiency. Figure 1 demonstrates the research process details of the nanotips used in THz s-SNOM. An excellent nanotip geometry design can reach an extreme spatial resolution while maintaining the near-field couple efficiency. And, the optimized nanotip needs an ideal incident field condition to achieve maximum performance. The Au nanotips and the Au surface (or Al_2O_3 surface) are described by Drude model with plasma frequency $\omega_{pl} = 2\pi \times 2100$THz, and the collision frequency $\gamma = 2\pi \times 50$THz [23]. The nanotip's length is 17μm. The nanotip's apex radius is 0.5~500nm. The cone angle is 10~40°.

3. Result and Discussion

Research on THz s-SNOM simulation primarily relies on point dipole models and finite-dipole models, in which the most prominent feature is that the nanotip apex is simplified into a sphere [24–27]. This paper further extends this model by simplifying the nanotip into a cone.

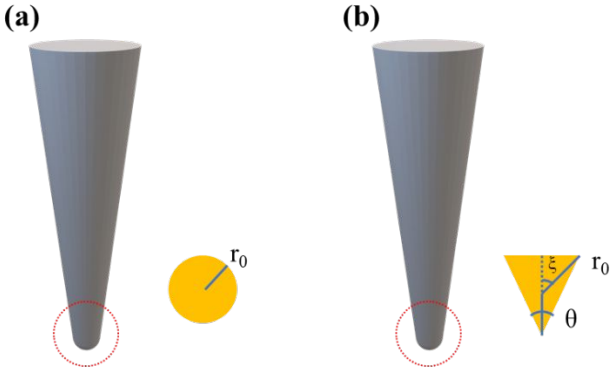

Figure 2 Two approximations methods of near-field nanotips. (a) The near-field nanotip is simplified as a sphere. (b) The near-field nanotip is simplified as a cone. θ is the cone angle of the nanotip, r_0 is the circumscribed circle radius, and ξ=θ.

In Figure 2 (a), the traditional dipole moment model simplifies the nanotip into a sphere. In Figure 2 (b), this article extends this model by simplifying the nanotip into a cone (The illustration shows the cross-section of a cone). θ is the cone angle of the nanotip, r_0 is the circumscribed circle radius. The cone cross-section is divided into three isosceles triangles to simplify calculations, thereby $\xi = \theta$. The effective polarizability of near-field coupling can be expressed as [28]:

$$\alpha_{eff} = \alpha\beta \tag{7}$$

α represents the effective polarizability of the nanotip irradiated by incident field, while β denotes the effective polarizability of mirror dipoles produced by the sample surface [28,29].

$$\beta = \frac{\varepsilon_{sample} - 1}{\varepsilon_{sample} + 1} \tag{8}$$

The polarizability α of a cone can be written as:

$$\alpha(\omega) = 8\pi\varepsilon_o r_o^3 f_e(\omega)(sin(\xi))^2(1 + cos(\xi)) \tag{9}$$

where $\varepsilon(\omega)$ is the dielectric function of the tip and ε_0 is the dielectric environment of the cone. $f_e(\omega)$ is the complex field-enhancement factor. According to the image diploe approximation, the image dipole has polarizability $\alpha\beta$ and is located at $-(d+r_0)$. r_0 represents the radius of the outer tangent circle of the cone. d is the nanotip-sample surface distance.

The equation 7 and 8 indicates that the near-field effective polarizability is comprised of nanotip's polarization and mirror dipole polarization. The intensity of the mirror dipole polarization is closely related to the sample material dielectric constant. The near-field enhancement effect of Au-Au system is greater than that of Au-Al_2O_3 system, the reason is that Au has a larger dielectric constant. Furthermore, the localized field spatial distribution depends on the near-field polarization at the nanotip apex. As the cone angle increases, the near-field polarization increases, resulting in a larger focusing spot diameter at the apex of the nanotip.

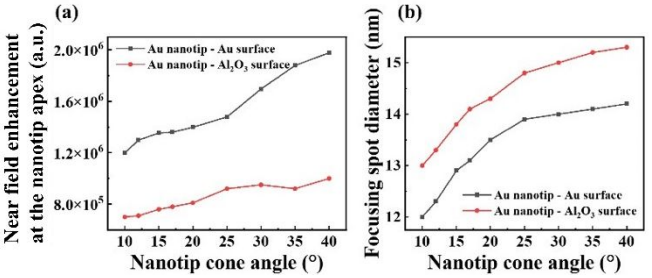

Figure 3. The evolution trend of the localized field enhancement at the nanotip apex and the FWHM of the focus diameter are influenced by Nanotip's cone angle. (a) Field enhancement at the nanotip's apex on two materials surfaces. (b) Focusing spot diameter at the nanotip's apex on two materials surfaces.

Figure 3 describes two near-field systems which are the Au nanotips-Au surface system and the Au nanotips-Al_2O_3 system respectively. In the Au nanotip-Au surface system, as the cone angle of the probe tip is varied from 10° to 40°, there is a 1.6-fold increase in localized field enhancement at the probe's apex and a corresponding 1.2-fold increase in the diameter of the focusing spot at this apex. In Au nanotip-Al2O3 surface system, as the cone angle of the probe tip is varied from 10° to 40°, there is a 1.1-fold increase in localized field enhancement at the probe's apex, and a corresponding 1.2-fold increase in the diameter of the focusing spot at this apex. Although the spatial resolution and the local field enhancement in different nanotip-sample systems are different, the overall trend is the same.

Figure 4 shows the dipole moment and focus point diameter of the focus points for several nanotips that are statically placed at a distance above the sample. Nanotips' parameters are as follows: nanotips' apex radius 5, 100, and 250nm, cone angle 20°, length 17 μm, and the nanotips-to-sample distance h = 5~1000 nm. Nanotip-sample dielectric system's dipole moment according to [28,29]:

$$\mathbf{p} = \alpha\left[\mathbf{E}_o + \mathbf{E}_{\text{image}}\right] \equiv \alpha_{\text{eff}}\mathbf{E}_o \tag{10}$$

α_{eff} is the effective polarizability, and $\boldsymbol{E_0}$ is the incident field. The effective polarizability is shown as follow:

$$\alpha_{\text{eff}} = \frac{\alpha[1-\beta]}{1-\alpha\beta/\left[32\pi\varepsilon_o\left(d+r_o\right)^3\xi\right]} \tag{11}$$

$\boldsymbol{\alpha}$ is the nanotips' polarization response of the incidence wave. $\boldsymbol{\beta}$ is the quasi-static Fresnel-reflection coefficient. From equations 11, the near-field couple efficiency depends on the nanotip-sample distance. Meanwhile, the increased near-field interaction changes the electric charge distribution below the nanotip. When the nanotip-sample distance decreases, the local surface charge density is drastically increased in this region, leading to stronger confinement, which reduces the focus point diameter of the localization field.

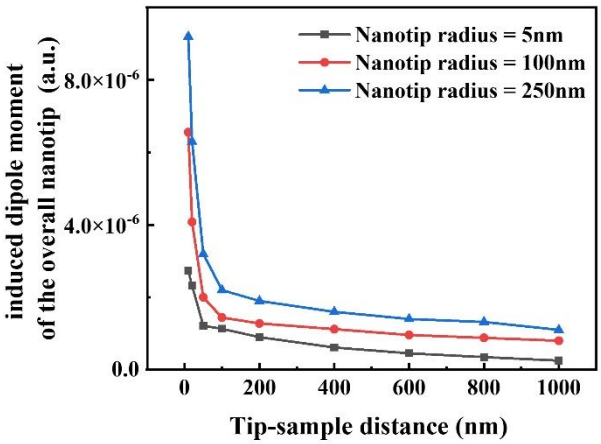

Figure 4. The evolution trend of the near field induced dipole moment of the overall nanotip is influenced by Nanotip apex-sample surface distance.

Systematically study the influence of the nanotips' apex radius on the near field couple efficiency and the spatial resolution is shown in Figure 5, in which the nanotip's geometry parameters are set as follows: the cone angle is 20°, the nanotips' length is 17 μm. In

Figure 5(a), the increase of the near field enhancement at the nanotip apex can be achieved by reducing the nanotip's radius. This simulation result is consistent with equations 10 and 11, a smaller nanotip apex radius leads to a larger near-field enhancement at the nanotip apex.

However, in Figure 5(b), the increased field enhancement at a smaller nanotip's apex doesn't result in an increased induced dipole moment of the overall nanotip. The specific analysis is as follows. The dipole moment of the overall nanotip reflects the current density integration of each cross-section along the z-direction of the nanotip, thereby comprehensively representing the scattered field generated by the nanotip. The scattering field and the induced dipole moment are shown as [30]:

$$E_{\text{scat}} \propto p = \left| \iint_S \sigma_S z \, \mathrm{d}S \right| \tag{12}$$

p is the dipole moment, σ_s is the surface charge density, z is the vertical position along the nanotip, and S is the surface cross-section area. The decreasing near-field enhancement at the nanotip apex for a larger apex radius is more than compensated by the larger near-field interaction area. Therefore, the induced dipole moment of the overall nanotip is increased when the nanotip apex radius increases.

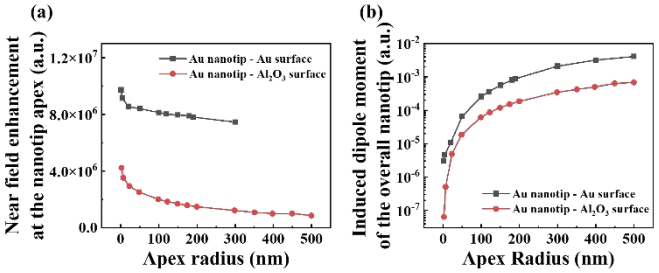

Figure 5. The evolution trend of the near field localized field enhancement at the nanotip apex and the FWHM of the focus diameter are influenced by Nanotip apex radius. (a) Field enhancement distribution at the nanotip's apex on two materials surfaces. (b) Dipole moment distribution of the overall nanotip on two materials surfaces.

Apart from the scattering nanotip's geometry, the incident field polarization is also influencing the near field couple efficiency. The relationship between the scattering field I and the incident field polarization can be simplified present as:

$$I(\theta) \propto \sin^2(\pi/2 - \theta) \tag{13}$$

θ is the included angle between the nanotip and the polarization of the incident THz wave [31]. From the equation 13, the near field polarization reaches maximum when the electric field vector of the incident wave has parallel to the nanotip. As it is shown in the Figure 6, the field enhancement of the focus point scattered by the nanotips is maximum when the incident field polarization is parallel to the nanotip. Although the incident field polarization influences the near field couple efficiency, the spatial resolution is independent of the incident field polarization as it is shown in the Figure 6.

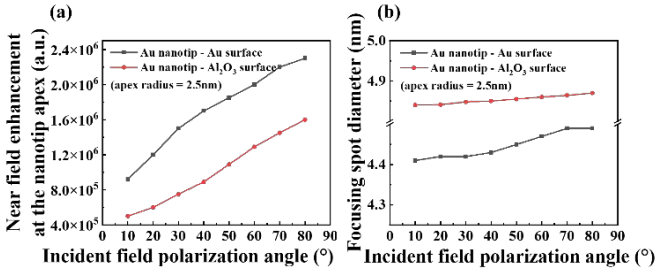

Figure 6. The evolution trend of the near field localized field enhancement at the nanotip apex and the FWHM of the focus diameter are influenced by incident field polarization status. (a) Field enhancement distribution at the nanotip's apex on two materials surfaces. (b) The evolution trend of the focusing spot diameter at the nanotip's apex with the incident field polarization.

For reasons similar to those mentioned in equation 7 and 8, the variations in near-field coupling efficiency and near-field focusing spot among different nanotip-sample systems in Figure 6 are attributed to the differences in the dielectric constants of the sample materials. The near-field enhancement effect of Au-Au system is greater than that of Au-Al_2O_3 system, the reason is that Au has a larger dielectric constant. Furthermore, the localized field spatial distribution depends on the near-field polarization at the nanotip apex. As the incident field angle changes, the near-field polarization increases, resulting in a larger focusing spot diameter at the apex of the nanotip.

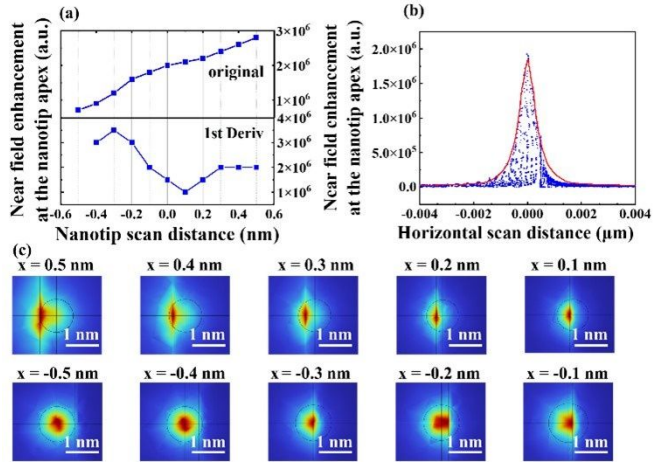

Figure 7. Numerical simulation of THz near field one-dimensional scanning. A tip with apex radius r = 0.5 nm and length 17 μm is placed above a sample consisting of Au on the left (x < 0 nm) and Al_2O_3 on the right (x > 0 nm) side. (a) Near field localized field enhancement evolution curve and corresponding derived curve. (b) electric near-field distribution in x = -0.5 nm. The red curve represents the Gaussian fitting curve of the near-field enhancement. (c) Electric field near-field distribution below the tip apex for different tip positions.

In the demonstration above, the various geometric parameters of the nanotip are comprehensively discussed. We can conclude that when only the influence of the nanotip's geometry on the THz near-field scanning spatial resolution, we can conclude that the nanotip apex radius is a primary factor. Therefore, we design a conical tip of 17 μm length and apex radius r = 0.5 nm was scanned above a sample modelled by Au on the left side, and Al_2O_3 on the right side to verify the THz-SNOM system's achievable ultimate spatial resolution [32]. The material boundary at x = 0 nm. The polarization of the input wave is parallel along the nanotips at 0.5 THz relative to the tip axis. The blue curve in Fig.7 (a) shows the result of field enhancement evolutionary trends at the nanotips' apex. The scanning spatial resolution depends on the nanotips' geometry and is described by the differential curve of the field enhancement evolutionary curve. By scanning the boundaries of two materials, the evolution of the field enhancement shows the spatial resolution is 0.5 nm. Fig.7 (b) shows the electric field near-field distribution in x = -0.5 nm (the nanotip is above the Au), which shows the focusing spot diameter is 0.5 nm. The near-field enhancement electric distribution of the nanotip's apex position conforms to a Gaussian distribution, exhibiting good symmetry. This is attributed to the optimization of the nanotip's parameters (nanotip's cone angle, nanotip's apex radius) and the near-field conditions (the nanotip's apex – sample surface distance).

We calculated the scattering coefficient at the apex of the nanotip apex to characterize the localized field enhancement at the nanotip apex. The interactions between the nanotip and the mirror dipoles define the total current density located at the nanotip in the presence of a sample and, therefore, the scattering coefficient [33]:

$$Scattering\ coefficient = \frac{E_{focus}}{E_{incident}} \propto 1 + \frac{\frac{f_0}{2}\beta}{1 - f_1\beta} = \frac{1.8\times10^6}{9.7\times10^3} \approx 185 \quad (14)$$

The nanotip apex and the mirror dipole create a situation akin to an optical resonator, enabling an increase in localized field enhancement at the nanotip apex through near-field interaction.

Figure 7 (c) shows the transverse scanning process continuously. The electric field near-field distribution shows significant changes when nanotips cross two materials' boundaries. Similar to equation 8, the difference in the different scattering boundaries can be attributed to the variation of the local-dielectric function of the sample based on the method of image charges.

The near field couple efficiency of the nanotips depends on the field enhancement and dipole moment distribution in the nanotip's apex, which can be described as effective polarizability. The scattering signal is influenced by nanotip geometry, nanotip sample distance, local dielectric properties of materials, and the polarization of the incidence wave. The near field scattering signal characterizes dielectric properties of the local materials by scanning the structure of the material and controlling the other factors unchanged. We improve the resolution to 0.5nm with 0.5THz (λ = 600 μm) by optimizing the nanotips' geometry, nanotip's apex to sample surface distance and incident field polarization. The optimization of the nanotips' geometry can noticeably improve the spatial resolution, especially for specific incident wavelengths. This method can provide the optimized nanotip parameters and assist the search for the balance parameters between the near field couple efficiency and spatial resolution. The nanotip design process and method mentioned in this paper provide a new method for improving the spatial resolution of THz s-SNOM.

Furthermore, we provide a brief overview of the nanotip fabrication process, which varies depending on the desired apex radius of the nanotips. The high-resolution nanotip fabrication can be categorized into two methods. The first method focuses on refining the apex of the nanotip to achieve a radius of approximately 3 nm or less. The secondary approach involves the growth of an additional nanotip, composed of high-density carbon, at the summit of the original nanotip pyramid. Consequently, the extra-nanotip extensions can be crafted with apex radius as fine as 1 nm or even less, further enhancing the precision and resolution of the nanotips [34–36]. The fabrication process of the conventional nanotip (apex radius 10nm~500nm) is based on photolithography and chemical etch. The nanotip's geometry is defines by the photolithography and the protective layer is removed by chemical etching [37].

4. Conclusion

In conclusion, ultrahigh resolution terahertz near-field scattering nanotips are investigated. The nanotip's geometry (cone angle, and apex radius), incident field, and local material dielectric constant are comprehensively considered to obtain the optimal parameters. From the perspective of the nanotip's geometry, the spatial resolution and the near-field couple efficiency mainly depend on the nanotip's apex radius and distance between the apex and sample surface. Other parameters such as the polarization of the incident field and the sample surface materials

mainly influence the near-field couple efficiency, but they don't change the spatial resolution significantly. Finally, this letter presents a feasible model to design optimal parameters of THz near-field scattering nanotip with 0.5 nm (λ/1200000) spatial resolution, while maintaining an excellent near-field couple efficiency ($185E_{incidenct}$). This method describes the nanotip's electromagnetic response in the near-field and provides a feasible method for designing the nanotip of the THz s-SNOM system.

Funding: The authors would like to thank the funding support from the National Natural Science Foundation of China (12061131010, 12074198)

Reference

[1]C. Koral, M. Fantauzzi, C. Imparato, G. P. Papari, B. Silvestri, A. Aronne, A. Andreone, and A. Rossi, *Defects in the Amorphous–Crystalline Evolution of Gel-Derived TiO $_2$*, J. Phys. Chem. C **124**, 23773 (2020).
[2]C. Koral et al., *Multi-Pass Free Electron Laser Assisted Spectral and Imaging Applications in the Terahertz/Far-IR Range Using the Future Superconducting Electron Source BriXSinO*, Front. Phys. **10**, 725901 (2022).
[3]R. Zheng, Y. Liu, L. Ling, Z. Sheng, Z. Yi, Q. Song, B. Tang, Q. Zeng, J. Chen, and T. Sun, *Ultra Wideband Tunable Terahertz Metamaterial Absorber Based on Single-Layer Graphene Strip*, Diamond and Related Materials **141**, 110713 (2024).
[4]R. I. Stantchev, J. C. Mansfield, R. S. Edginton, P. Hobson, F. Palombo, and E. Hendry, *Subwavelength Hyperspectral THz Studies of Articular Cartilage*, Sci Rep **8**, 6924 (2018).
[5]L. He, Y. Yi, J. Zhang, X. Xu, B. Tang, G. Li, L. Zeng, J. Chen, T. Sun, and Z. Yi, *A Four-Narrowband Terahertz Tunable Absorber with Perfect Absorption and High Sensitivity*, Materials Research Bulletin **170**, 112572 (2024).
[6]W. Lu, Z. Yi, J. Zhang, X. Xu, B. Tang, G. Li, L. Zeng, J. Chen, and T. Sun, *A Tunable Broadband Absorber in the Terahertz Band Based on the Proportional Structure of a Single Layer of Graphene*, Diamond and Related Materials **140**, 110481 (2023).
[7]A. J. Huber, F. Keilmann, J. Wittborn, J. Aizpurua, and R. Hillenbrand, *Terahertz Near-Field Nanoscopy of Mobile Carriers in Single Semiconductor Nanodevices*, Nano Lett. **8**, 3766 (2008).
[8]F. Huth, A. Govyadinov, S. Amarie, W. Nuansing, F. Keilmann, and R. Hillenbrand, *Nano-FTIR Absorption Spectroscopy of Molecular Fingerprints at 20 Nm Spatial Resolution*, Nano Lett. **12**, 3973 (2012).
[9]C. Liewald, S. Mastel, J. Hesler, A. J. Huber, R. Hillenbrand, and F. Keilmann, *All-Electronic Terahertz Nanoscopy*, Optica **5**, 159 (2018).
[10]A. S. McLeod, P. Kelly, M. D. Goldflam, Z. Gainsforth, A. J. Westphal, G. Dominguez, M. H. Thiemens, M. M. Fogler, and D. N. Basov, *Model for Quantitative Tip-Enhanced Spectroscopy and the Extraction of Nanoscale-Resolved Optical Constants*, Phys. Rev. B **90**, 085136 (2014).
[11]F. Huth, A. Chuvilin, M. Schnell, I. Amenabar, R. Krutokhvostov, S. Lopatin, and R. Hillenbrand, *Resonant Antenna Probes for Tip-Enhanced Infrared Near-Field Microscopy*, Nano Lett. **13**, 1065 (2013).
[12]S. Mastel, M. B. Lundeberg, P. Alonso-González, Y. Gao, K. Watanabe, T. Taniguchi, J. Hone, F. H. L. Koppens, A. Y. Nikitin, and R. Hillenbrand, *Terahertz Nanofocusing with Cantilevered Terahertz-Resonant Antenna Tips*, Nano Lett. **17**, 6526 (2017).
[13]G. Gomila, G. Gramse, and L. Fumagalli, *Finite-Size Effects and Analytical Modeling of Electrostatic Force Microscopy Applied to Dielectric Films*, Nanotechnology **25**, 255702 (2014).
[14]H.-T. Chen, S. Kraatz, G. C. Cho, and R. Kersting, *Identification of a Resonant Imaging Process in Apertureless Near-Field Microscopy*, Phys. Rev. Lett. **93**, 267401 (2004).
[15]F. Kuschewski, H.-G. Von Ribbeck, J. Döring, S. Winnerl, L. M. Eng, and S. C. Kehr, *Narrow-Band near-Field Nanoscopy in the Spectral Range from 1.3 to 8.5 THz*, Applied Physics Letters **108**, 113102 (2016).
[16]J. Belhassen, S. Glass, E. Teblum, G. A. Stanciu, D. E. Tranca, Z. Zalevsky, S. G. Stanciu, and A. Karsenty, *Toward Augmenting Tip-Enhanced Nanoscopy with Optically Resolved Scanning Probe Tips*, Adv. Photon. Nexus **2**, (2023).
[17]F. Lu, M. Jin, and M. A. Belkin, *Tip-Enhanced Infrared Nanospectroscopy via Molecular Expansion Force Detection*, Nature Photon **8**, 307 (2014).
[18]才家华 1 张保龙 2, 耿春艳 1 郝思博 3, 陈赛 1 4, and 吴晓君 1 4*, 铌酸锂强场太赫兹非线性时域光谱系统, (n.d.).
[19]J. Zhao et al., *Strong Spatial Confinement of Terahertz Wave inside Femtosecond Laser Filament*, ACS Photonics **3**, 12 (2016).
[20]H. Wang, L. Wang, and X. G. Xu, *Scattering-Type Scanning near-Field Optical Microscopy with Low-Repetition-Rate Pulsed Light Source through Phase-Domain Sampling*, Nat Commun **7**, 13212 (2016).
[21]W. Greiner, *Classical Electrodynamics* (Springer Science & Business Media, 2012).
[22]J. D. Jackson, *Classical Electrodynamics*, (1999).
[23]M. W. Klein, C. Enkrich, M. Wegener, and S. Linden, *Second-Harmonic Generation from Magnetic Metamaterials*, Science **313**, 502 (2006).
[24]X. Chen, Z. Yao, S. G. Stanciu, D. N. Basov, R. Hillenbrand, and M. Liu, *1Rapid Simulations of Hyperspectral Near-Field Images of Three-Dimensional Heterogeneous Surfaces*, Opt. Express **29**, 39648 (2021).
[25]X. Chen, Z. Yao, Z. Sun, D. N. Basov, R. Hillenbrand, and M. Liu, *2Rapid Simulations of Hyperspectral Near-Field Images of Three-Dimensional Heterogeneous Surfaces – Part II*, (n.d.).
[26]Z. Peng, D. Zhang, S. Ge, and J. Meng, *Quantitative Modeling of Near-Field Interactions in Terahertz Near-Field Microscopy*, Applied Sciences **13**, 3400 (2023).
[27]D. Datz, G. Németh, L. Rátkai, Á. Pekker, and K. Kamarás, *Generalized Mie Theory for Full-Wave Numerical Calculations of Scattering Near-Field Optical Microscopy with Arbitrary Geometries*, Physica Rapid Research Ltrs **18**, 2300370 (2024).
[28]A. Cvitkovic, N. Ocelic, and R. Hillenbrand, *Analytical Model for Quantitative Prediction of Material Contrasts in Scattering-Type near-Field Optical Microscopy*, Opt. Express **15**, 8550 (2007).
[29]L. Novotny and S. J. Stranick, *NEAR-FIELD OPTICAL MICROSCOPY AND SPECTROSCOPY WITH POINTED PROBES*, Annu. Rev. Phys. Chem. **57**, 303 (2006).
[30]C. Maissen, S. Chen, E. Nikulina, A. Govyadinov, and R. Hillenbrand, *Probes for Ultrasensitive THz Nanoscopy*, ACS Photonics **6**, 1279 (2019).
[31]L. Aigouy, A. Lahrech, S. Grésillon, H. Cory, A. C. Boccara, and J. C. Rivoal, *Polarization Effects in Apertureless Scanning Near-Field Optical Microscopy:?An Experimental Study*, Opt. Lett. **24**, 187 (1999).
[32]B. Kusnetz, J. Belhassen, D. E. Tranca, S. G. Stanciu, S.-R. Anton, Z. Zalevsky, G. A. Stanciu, and A. Karsenty, *Generic Arrays of Surface-Positioned and Shallow-Buried Gold Multi-Shapes as Reference Samples to Benchmark near-Field Microscopes. Part 1: Applications in s-SNOM Depth Imaging*, Results in Physics **56**, 107318 (2024).
[33]X. Guo, K. Bertling, and A. D. Rakić, *Optical Constants from Scattering-Type Scanning near-Field Optical Microscope*, Applied Physics Letters **118**, 041103 (2021).
[34]J. Tang, G. Yang, Q. Zhang, A. Parhat, B. Maynor, J. Liu, L.-C. Qin, and O. Zhou, *Rapid and Reproducible Fabrication of Carbon Nanotube AFM Probes by Dielectrophoresis*, Nano Lett. **5**, 11 (2005).
[35]Sheng, Czajkowsky, and Shao, *AFM Tips: How Sharp Are They?*, Journal of Microscopy **196**, 1 (1999).
[36]N. R. Wilson and J. V. Macpherson, *Carbon Nanotube Tips for Atomic Force Microscopy*, Nature Nanotech **4**, 483 (2009).
[37]S. Krämer, R. R. Fuierer, and C. B. Gorman, *Scanning Probe Lithography Using Self-Assembled Monolayers*, Chemical Reviews **103**, 4367 (2003).